

Perspectives on Advances in Quantum Dot Lasers and Integration with Si Photonic Integrated Circuits

Chen Shang,^{*,#} Yating Wan,[#] Jennifer Selvidge, Eamonn Hughes, Robert Herrick, Kunal Mukherjee, Jianan Duan, Frederic Grillot, Weng W. Chow, and John E. Bowers



Cite This: <https://doi.org/10.1021/acsphotonics.1c00707>



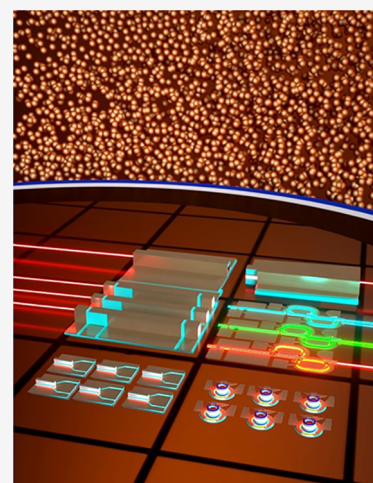
Read Online

ACCESS |

Metrics & More

Article Recommendations

ABSTRACT: Epitaxially grown quantum dot (QD) lasers are emerging as an economical approach to obtain on-chip light sources. Thanks to the three-dimensional confinement of carriers, QDs show greatly improved tolerance to defects and promise other advantages such as low transparency current density, high temperature operation, isolator-free operation, and enhanced four-wave-mixing. These material properties distinguish them from traditional III–V/Si quantum wells (QWs) and have spawned intense interest to explore a full set of photonic integration using epitaxial growth technology. We present here a summary of the most recent developments of QD lasers grown on a CMOS-compatible (001) Si substrate, with a focus on breakthroughs in long lifetime at elevated temperatures. Threading dislocations are significantly reduced to the level of $1 \times 10^6 \text{ cm}^{-2}$ via a novel asymmetric step-graded filter. Misfit dislocations are efficiently blocked from the QD region through well-engineered trapping layers. A record-breaking extrapolated lifetime of more than 200000 hours has been achieved at 80 °C, forecasting that device reliability is now entering the realm of commercial relevance and a monolithically integrated light source is finally on the horizon.



KEYWORDS: quantum dot (QD), Si photonics, on-chip lasers, lifetime, monolithic integration, heteroepitaxial growth

Internet Protocol traffic has experienced a compound annual growth rate of 27% in the past few years, in which almost 75% of the data traffic resides within the data center.^{1,2} Leveraging well-established processing in Si-based microelectronics, Si photonics is expected to meet this soaring global demand for low power and high bandwidth density optical interconnects.^{3,4} Both Si and its native oxide are transparent in the commercially important datacom and telecom wavelength ranges and can form high-index contrast waveguides ideally suited for highly integrated photonic integrated circuits (PICs).^{5–7} A variety of high-performance passive components have been demonstrated on 300 mm Si wafers.⁸ Yet, due to the indirect bandgap of Si and Ge, realizing on-chip light sources requires integrating high quality III–V gain materials onto the existing Si photonic platforms. Compared to earlier hybrid integration where precise laser-chip alignment is needed at the final packaging stage, heterogeneous integration via wafer bonding has greatly simplified the integration process and provides the prospect for scalable manufacturing. Through a decade of nonstop innovations in academia and industry, heterogeneous integration is currently reaching maturity, achieving mass commercial production lines.^{5,9} However, the cost and the size of III–V

substrates and the complex bonding processes limit the economies of scale.

Monolithic integration through direct epitaxial growth is more economically favorable and provides a better heat-dissipation capability. Yet, the performance of epitaxially grown quantum well (QW) devices on Si fall far behind native substrate devices due to the crystalline defects generated during the heteroepitaxial growth. QDs, first introduced in 1982 by Arakawa and Sakaki,¹⁰ are important because the strong strain field induced by QDs hinders the in-plane movement of dislocations.¹¹ Besides the defect insensitivity,^{12,13} QDs have numerous performance advantages over QWs, including lower threshold current, higher temperature operation, a near zero line width enhancement factor and, thus, isolator-free stability, ultrafast gain recovery, and enhanced four-wave mixing. Exciting technological advances have been

Received: May 11, 2021

Revised: July 29, 2021

Accepted: July 30, 2021

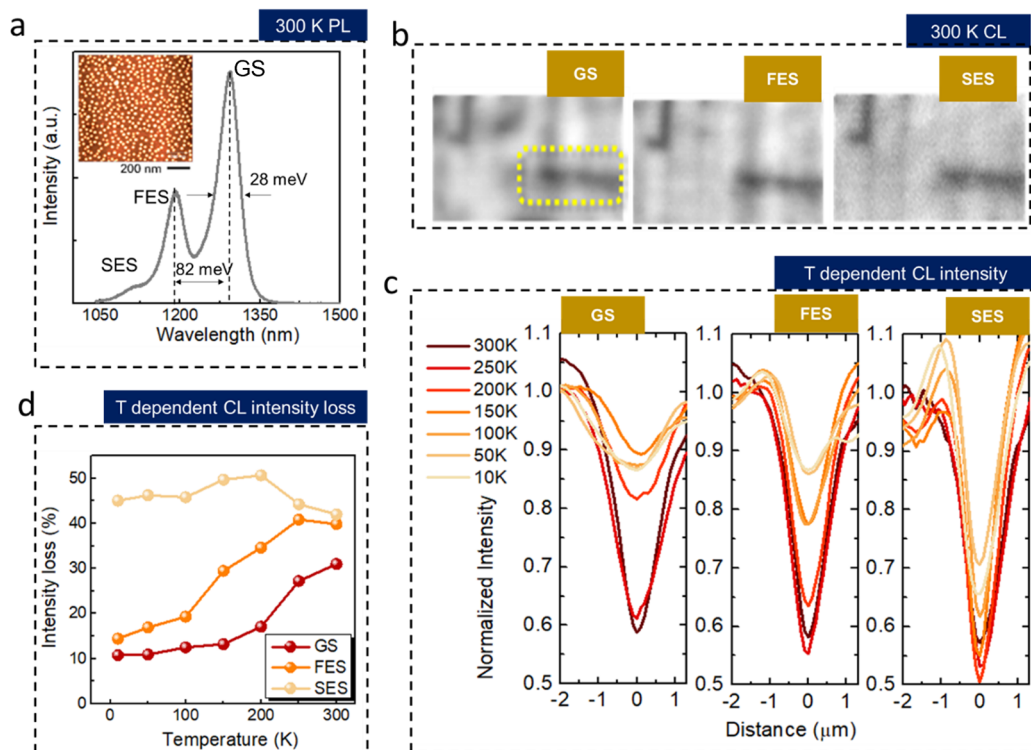


Figure 1. (a) Room-temperature PL spectrum of InAs QDs grown on a GaAs substrate, with a ground state peak wavelength of 1293 nm. The energy separation between the ground state and the first excited state is 82 meV. The inset shows the atomic force microscopy (AFM) scan of the exposed surface dots, where the surface dot density is about $6 \times 10^{10} \text{ cm}^{-2}$. (b) Filtered CL maps for different transitions at 300 K. (c) Temperature-dependent CL intensity line scan across the identified MD, located at the origin, in different transitions. (d) Extracted average intensity loss with respect to the temperature for different transitions. (b)–(d) are reproduced with permission from ref 24. Copyright 2019 AIP Publishing.

made in the field of epitaxially grown QD devices on Si, as described in several previous review articles, summarizing the evolution of device performance, and efforts in developing CMOS compatible epitaxial platform on (001) Si.^{11,14–19}

In this Review, we will present the most recent advances in monolithically integrated QD devices on a Si photonic platform, with a focus on breakthroughs in a long lifetime at elevated temperatures. After a brief introduction of the fundamental advantages of QDs, we will summarize several technological breakthroughs at the device and platform levels. Specifically, through the novel management of crystalline defects, the most recent breakthroughs in high temperature CW operation will be described. Finally, we end by providing a high-level summary of the different generations of lasers and aging results and discussing the prospects in obtaining a monolithic integration in real-world applications.

FUNDAMENTAL ADVANTAGES OF THE QD ACTIVE REGION

Discrete Density of States. Semiconductor QDs are “artificial atoms” that confine carriers in all three dimensions. Theoretically, the band offsets between the narrow bandgap dot material and the surrounding matrix gives rise to full discretization of the energy levels and delta function-like density of states.²⁰ But, in practice, self-assembled QDs grown via the Stranski–Krastanov (S–K) growth mode experience inhomogeneous broadening due to growth variations and are connected through a thin wetting layer.²¹ Figure 1a shows the example room temperature photoluminescence (PL) spectrum

of InAs QDs grown on a GaAs substrate with labeled ground state (GS), the first excited state (FES), and the second excited state (SES). The measured full-width-at-half-maximum (fwhm) of the ground state peak is 28 meV, which translates to an inhomogeneous broadening Δ_{inh} of approximately 13 meV.²² This value of Δ_{inh} for typical self-assembled QDs is small compared to the energy separation between the quantum states (around 80 meV).^{22,23} Thus, the states in the QD ensemble remain discrete. With this discrete density of states, the carrier density required for population inversion is reduced. Therefore, the short carrier lifetime of the ground state supports a high level of radiative optical transitions per unit volume. This mechanism contributes to a low threshold carrier density.

Reduced Carrier Lateral Diffusion. Naturally localized carriers in QDs also contribute to strongly suppressed carrier diffusion compared to that of QWs.²⁵ Reduced lateral carrier diffusion length is known to minimize problems associated with surface recombination and, thus, facilitate device miniaturization without imposing a penalty on the lasing threshold.²⁶ Carrier diffusion length can be measured with the cathodoluminescence (CL) intensity loss near a misfit dislocation (MD). Examples of 10 kV CL maps done at 300 K on an epitaxially grown InAs QD material on Si are shown in Figure 1b, filtered for the GS, FES, and SES. A typical MD was identified (circled in yellow), and the normalized intensity profiles across the MD are shown in Figure 1c. The extracted intensity loss with respect to temperature is summarized in Figure 1d. Compared to a GaAs or an InGaAs QW, where carriers have a diffusion length on the order of $2 \mu\text{m}$ at 10 K,²⁶

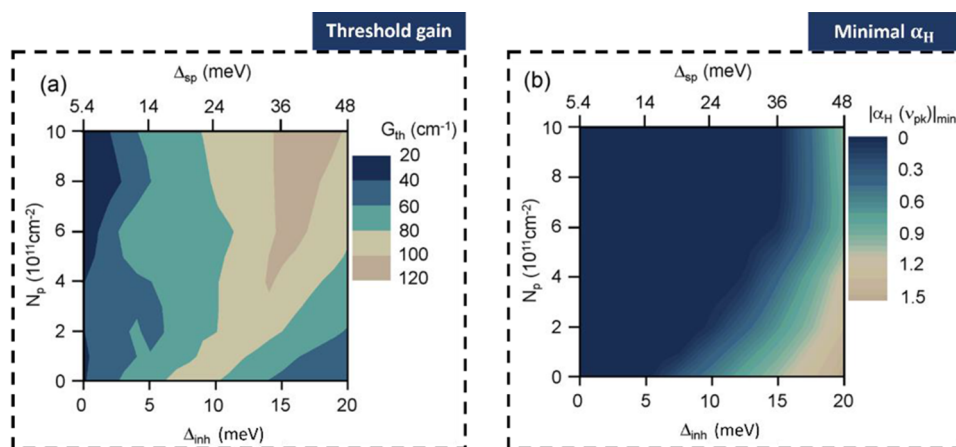


Figure 2. Combination map between Δ_{inh} , N_p , and G_{th} for (a) $|\alpha_{\text{H}}(\nu_{\text{pk}})|_{\text{min}}$ and (b) $|\alpha_{\text{H}}(\nu_{\text{pk}})|_{\text{min}}$ obtainable with these combinations. The figures are reprinted with permission from Chow, W. W. et al. On Quantum-Dot Lasing at Gain Peak with Line Width Enhancement Factor $\alpha_{\text{H}} = 0$. *APL Photonics* 2020, 5 (2), 0–6, <https://doi.org/10.1063/1.5133075>. Licensed under a Creative Commons Attribution (CC BY) license.

the measured carrier diffusion length in an InAs QD structure is as low as $0.5 \mu\text{m}$ at room temperature, as is evident from Figure 1c,²⁴ consistent with earlier research.²⁵

With this much reduced diffusion length in QDs, Fabry–Pérot (FP) QD lasers grown on Si showed that reducing the ridge width shows a continuous decrease of threshold currents down to a $2 \mu\text{m}$ ridge width with no sign of threshold current density increase.²⁷ Microring resonators fabricated from the same material demonstrate monotonically decreased threshold currents with the reduction of the ring radius.²⁸ Threshold currents below 1 mA were achieved with a radii as small as $4 \mu\text{m}$.²⁹ Decreased carrier diffusion length also reduces the sensitivity to crystalline defects. Since crystalline defects are unavoidable in epitaxially grown III–V material on Si, this makes QD emitters an ideal candidate for monolithic light source integration. Another important aspect that can be seen from Figure 1c,d is that the excited state transitions are more affected by the nearby defects due to higher carrier escape rates. Thus, maintaining a ground state operation is essential for reliable and high performance epitaxially grown devices.

Improved Temperature Dependence. As the energy separation between the quantum states are a few times larger than kT at room temperature, the threshold current of QD active region is expected to be insensitive to the temperature change. Yet, due to recombination in the surrounding materials and neutrality violation, real QD device threshold does experience noticeable temperature dependence at high enough temperatures.²⁰ In that case, the thermal escape rate of carriers in QDs increases exponentially with temperature and is accompanied by a sharp increase in the threshold current.^{29–33} Still, a characteristic temperature (T_0) as high as 175 K and CW operation to at least $220 \text{ }^\circ\text{C}$ have been obtained in a packaged InAs QD laser grown on a native GaAs substrate.³⁴ Optimizing the laser epi design to minimize charge neutrality violation and recombination outside of the QD active region can further reduce the temperature sensitivity. Recently, a T_0 as high as 167 K has been extracted from epitaxially grown and unpackaged devices on (001) Si. The maximum lasing temperature is $>110 \text{ }^\circ\text{C}$. The details for such epi will be discussed in the section **Demonstration of High Temperature Robust Operation**.

Reduced Line Width Enhancement Factor. Another important advantage of QDs is the small line-width enhance-

ment factor, α_{H} , which is crucial for applications ranging from datacom and telecom to LiDAR and chemical sensing. The α_{H} can be expressed as a function of the carrier-induced refractive index δn , gain G , and the carrier density N_e ,²² and are closely related to both the laser line width, $\Delta\nu$, and the critical feedback level, f_{crit} .³⁵

$$\alpha_{\text{H}} = -2K \frac{d(\delta n)}{dN_e} \left(\frac{dG}{dN_e} \right)^{-1} \quad (1)$$

$$\Delta\nu = \Delta\nu_{\text{ST}}(1 + \alpha_{\text{H}}^2) \quad (2)$$

$$f_{\text{crit}} = C \left(\frac{1 + \alpha_{\text{H}}^2}{\alpha_{\text{H}}^4} \right) \quad (3)$$

Here, $\Delta\nu_{\text{ST}}$ is the modified Schawlow–Townes line width, and C is a structural constant. An α_{H} value in the range of 2–5 for QW lasers^{36–38} results in a broadened line width and a critical feedback level smaller than 0.01% of the output power before coherence collapse.³⁹ Both effects require additional components in the package. QD lasers have a lower α_{H} as the carriers are confined in individual potential wells, and changes in the index or gain are localized. Yet, due to inhomogeneous broadening in the self-assembled QDs, the off-resonance QD subgroups would contribute to an increase in α_{H} .³⁵ To obtain low α_{H} values, it is important to reduce Δ_{inh} , as well as improve the differential gain. With optimized growth conditions, state-of-the-art self-assembled QDs have an extracted Δ_{inh} as low as 10 meV. By adding extra holes through p -type modulation doping ($p\text{MD}$), the compensated thermalization of the less-confined holes contributes to enhanced population inversion and, thus, much improved gain in the material.⁴⁰ Figure 2a shows the necessary combinations of Δ_{inh} , p -doped density N_p , and threshold gain G_{th} to achieve lasing at the gain peak with the minimum absolute value of α_{H} ($|\alpha_{\text{H}}(\nu_{\text{pk}})|_{\text{min}}$). Figure 2b shows the resulting $|\alpha_{\text{H}}(\nu_{\text{pk}})|_{\text{min}}$ with those combinations. It is important to note that, in Figure 2b, there is a sizable region to reach zero α_{H} at the gain peak ($\alpha_{\text{H}}(\nu_{\text{pk}}) = 0$), which can be obtained with a subset of Δ_{inh} , N_p , and G_{th} that are reachable in present QD lasers. This parametric study, supported with experiments, suggests that QD lasers may be configured to operate with vanishing α_{H} operation.²²

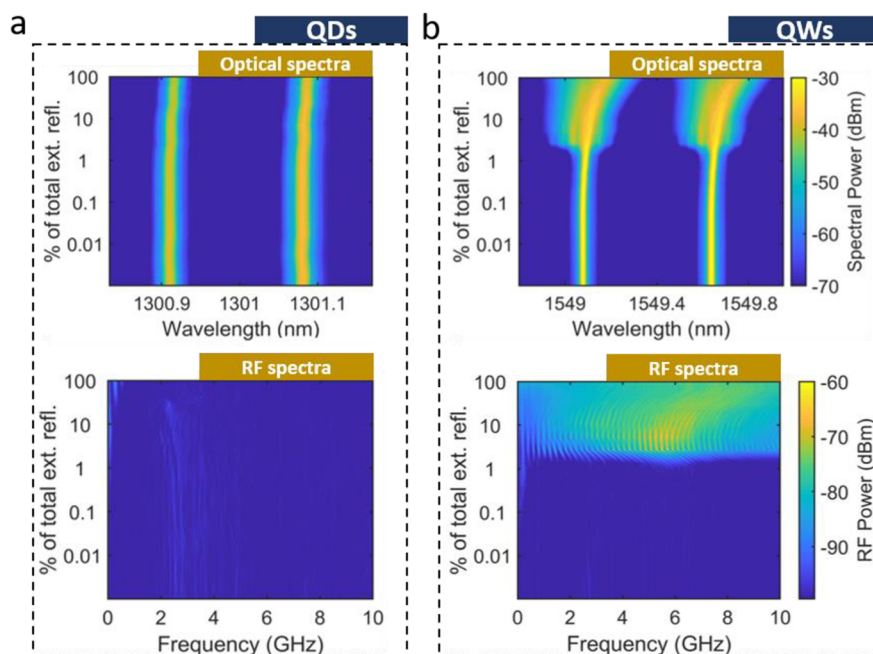


Figure 3. (a) Optical (upper) and RF (lower) spectra of the QD lasers on Si as a function of the feedback level. (b) Optical (upper) and RF (lower) spectra of the QW lasers as a function of the feedback level. The maps were obtained at an injection level of $3 \times I_{th}$.⁴²

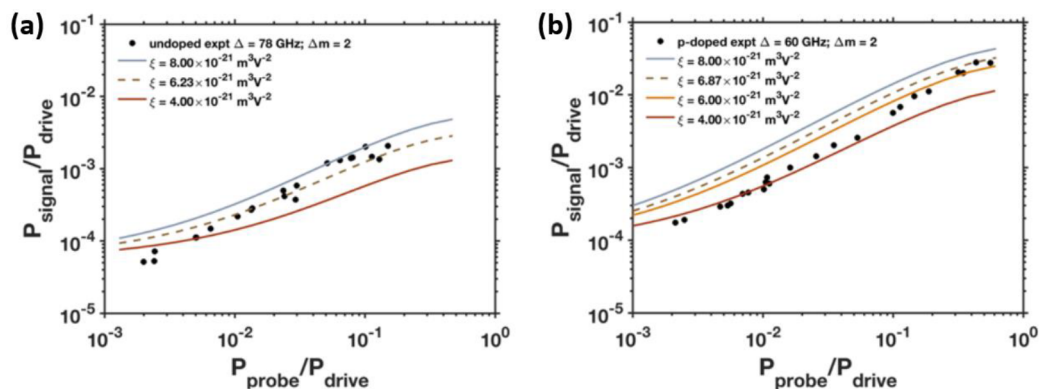


Figure 4. Normalized signal power versus probe power in a probe-drive laser experiment for (a) undoped and (b) *p*-doped lasers. The frequency detuning, Δ , corresponds to the same mode number difference. Dashed lines are calculated from multimode laser theory and the solid lines are calculated from selected ξ values. The figures are reprinted with permission from ref 45. Licensed under a Creative Commons Attribution (CC BY) license.

α_H values below unity at gain peak have been measured with the lowest reported value being 0.097 at a *p*-type modulation doping level equivalent to 20 extra holes per dot.^{22,35,41} FP lasers fabricated from the same QD material grown on Si have demonstrated an exceptional tolerance to optical feedback. As shown in Figure 3a, QD lasers on Si have only showed a small redshift of the modal wavelength up to 100% external reflection at $3 \times I_{th}$ in the optical spectra and no sign of nonlinear oscillations is observed in the RF response. On the contrary, just at a feedback level of 1.7%, the QW lasers experience coherence collapse with strong broadening of the modes and intense chaotic oscillations in the RF domain, as shown in Figure 3b.⁴² Similar results have been shown in a more recent study as well.⁴³ Such high tolerance to the optical feedback of QD lasers paves the way to achieve isolator-free photonic integrated circuit packaging in the future.

Enhanced Four Wave Mixing. Due to the symmetric gain spectrum of QDs under equilibrium state filling with a small

Δ_{inh} ($\Delta_{inh} < kT$), QD devices exhibit enhanced four-wave mixing (FWM) through third-order nonlinear interactions. Measured FWM conversion efficiencies on an InAs QD laser with *p*-type modulation doping are close to the theoretical limit from the first principal calculations.⁴⁴ Figure 4 shows the results of probe-drive laser experiments on InAs QD lasers grown on Si, for active regions with undoped and *p*-modulation doped spacer layers. The drive laser power was fixed and the probe-drive mode number difference, Δm , is 2 in both cases. The experimental results in both cases are bounded by a choice of net FWM coefficient, $\xi \equiv \frac{\chi^{(3)}}{g_s}$, between 4 and $8 \times 10^{-21} \text{ m}^3 \text{ V}^{-2}$, where $\chi^{(3)}$ is the third-order nonlinear susceptibility and g_s is the material gain. The gain in signal power is higher for lasers with a *p*-doped active region than those with an undoped active region, despite the same value of ξ . Duan et al. suggested that the gain competition and $\chi^{(3)}$

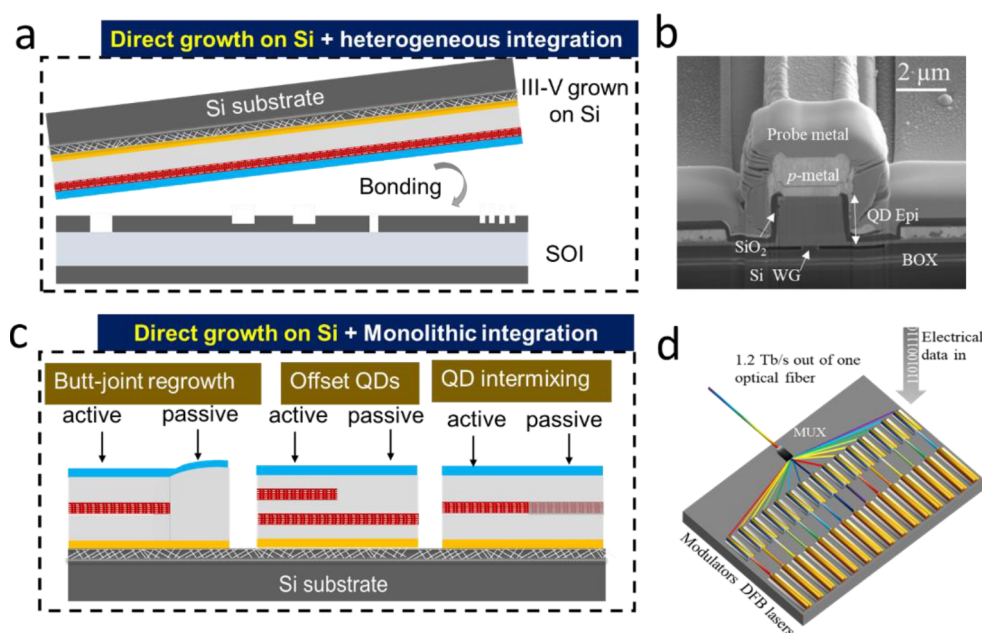


Figure 5. (a) Integration schemes to achieve heterogeneous integrated QD devices by direct epi growth. (b) Cross-sectional FIB-SEM image at the hybrid session for a heterogeneous integrated QD DFB laser. Reprinted with permission from ref 49. Copyright 2021 Wiley VCH. (c) Integration schemes to achieve monolithic integrated QD devices by direct epi growth. (d) A concept for a Si terabit transmitter utilizing monolithically integrated regrown QD-DFB EML. Reprinted with the permission from ref 50. Copyright 2020 Wiley VCH.

should be considered on equal footing when evaluating mode-locking performance.⁴⁴

Strong FWM is theorized to facilitate single-section mode-locked lasers (MLL), which have higher output power and simpler fabrication procedures compared to the two-section MLL with a saturable absorber.⁴⁶ Such devices have also been demonstrated experimentally.^{47,48} High-performing MLLs could greatly simplify the design of wavelength-division multiplexing (WDM) systems.

Integration. Parallel to the continual improvement of material quality and individual QD device performance on Si by epitaxial growth, intense efforts are also devoted to the development of fully integrated photonic circuits. Today, InP-based monolithic integration and Si photonics are the two major integration technologies in photonics. QD-based PICs on Si can thus be built upon what has been achieved through either monolithic or heterogeneous integration to both improved performance and reduced cost.

Heterogeneous Integration. To achieve low-loss active–passive coupling of III–V with Si waveguides, heterogeneous integration offers an elegant path, as shown in Figure 5a. Ever since the invention of the first prototype QW-based heterogeneous laser in 2006,⁵¹ it only took 10 years for Intel to announce the first commercial products. The successful commercialization of InP-based QW-based heterogeneous integration indicates that GaAs-based QDs for 1300 nm and InAs/InP QDs/quantum dashes⁵² for 1550 nm should be straightforward engineering, and some of the lessons can be leveraged, for example, efficient bonding strength, reliable operation, adoption by the CMOS production foundries, and efficient active–passive optical coupling. Changing from InP-based QW epi to GaAs-based QD epi requires different material systems and, thus, completely different device design, as well as process optimization. While research has been conducted actively in both heterogeneous QW lasers and QD

lasers, combining the two together is still at an embryonic stage.

The first demonstration of light coupling between QD lasers and Si waveguides was achieved by G. Kurczveil et al. in 2016.⁵³ Heterogeneous QD microring lasers on Si show low threshold currents comparable to that of the monolithic integrated ones (both at the level of submilliamp), but with a distinct advantage that efficient light output of ~ 0.6 mW can be coupled into the Si waveguide.^{29,54} However, microlasers have high thermal impedance, and heat sinking is more challenging for the heterogeneous ones due to the high thermal resistance introduced by the III–V-to-Si bonding layer and the buried oxide. Joule heating then limits the maximum operating temperature to 70 °C, which is lower than that of the monolithic integrated QD microring lasers (100 °C CW). Extra thermal shunt designs are required, and the buried oxide thickness needs to be optimized to maintain both the coupling efficiency and the thermal performance. Since the light is evanescently coupled between the QD active region and the Si waveguides, the laser cavity design and the gain active region can be separately optimized. By engineering the Si grating designs, rapidly increasing performance is shown in heterogeneously integrated QD DFB lasers: a side-mode-suppression ratio (SMSR) of 40 dB is achieved based on second order surface gratings,⁵⁵ a SMSR of 61 dB and a Lorentzian line width of 211 kHz is achieved based on a shallow etched first-order grating,⁵⁶ a SMSR of 60 dB and a Lorentzian line width of 26 kHz is achieved based on first-order side-hole gratings.⁴⁹ The Lorentzian line width of tens of kHz is low compared to the typical solitary QW laser line width of several megahertz, attributed to the much lower α_H of QDs. In addition, this value also significantly outperforms QD DFB lasers without a Si waveguide, that is, 480 kHz in ref 57, 1.275 MHz in ref 58, and 6 MHz in ref 59.

Similarly, the combinations of different Si external cavity designs and the QD active region prove to be effective ways to

simultaneously provides the tuning mechanism of the laser as well as the line width reduction. A tunable Mach–Zehnder interferometer (MZI), high-Q ring resonators, or a combination of them all serve well as this extended passive section. Using a Vernier dual-ring geometry and an additional wavelength filter in the form of an MZI, 52 nm tuning range, 58 dB SMSR, and 5.3 kHz Lorentzian line width have been achieved.⁶⁰ The tuning range and SMSR exceed the value of 16 nm and 45 dB obtained in a monolithic QD tunable laser with two all-active ring resonators coupled to a common FP cavity.⁶¹ The Lorentzian line width is also far better than that of the monolithic ones using a half-wave coupled cavity structure (716 kHz).⁵⁷ This shows a clear synergistic relationship between the capabilities of QDs and low-loss Si waveguides/cavities that gives rise to performance exceeding what is achievable with an all III–V system. A similar InAs/GaAs QD gain medium has also been used to make heterogeneous QD comb laser and a more sophisticated circuit design is enabled by integrating the QD comb lasers with SiGe avalanche photodetectors (APDs) on the same wafer.⁶² In this 10-channel transceiver link, aggregated 160 Gb/s error-free NRZ data transmission is obtained with an energy consumption of 3 pJ/bit. In the future, one can grow InAs QD gain material on Si and then bond onto a prepatterned SOI substrates. The large wafer-scale hetero-epitaxy growth of QD material on Si can significantly reduce the unit price of the gain material and solves the wafer size limit for wafer scale III–V to Si bonding, which is set by the maximum available size of InP wafers (150 mm diameter).

Monolithic Integration with All III–V Waveguides.

Since buffer layers between the QDs and the Si are thick, coupling between the epitaxial QD active region with the Si waveguides and the rest of the Si photonic library is challenging. Therefore, a kind of natural viewpoint is to establish a platform with all photonic functionalities solely in the QD-based stack, similar to InP-based monolithic integration and using the Si wafer as a pure handling substrate. This is schematically described in Figure 5c. The key to this approach is the combination of different bandgaps into one optical chip. Therefore, integration approaches such as regrowth, intermixing, and offset active regions that are widely used in the InP-based photonic circuits can be leveraged here.⁶³ Following this direction, a monolithic offset QD integration platform has been built enabling the formation of a laser cavity utilizing both a robust QD active region and versatile passive GaAs waveguide structures.⁶³ In this approach, GaAs/AlGaAs selective etch and linear taper designs are utilized to make transitions between the passive and active waveguides in the III–V epi stack. Since the active region was shifted upward from the center of the intrinsic region, the lower half of the intrinsic region can be utilized as a passive waveguide layer to form a laser cavity or other passive waveguide structures for light partitioning, routing, and switching purposes.

In a separate work, regrown QD distributed feedback (DFB) lasers have been demonstrated with temperature-stable, single-longitudinal-mode operation (side-mode suppression ratio of more than 50 dB) and a threshold current density of 440 A/cm².⁵⁰ The finite intraband relaxation time and gain saturation effect limit the direct modulation bandwidth of QD laser to 4–10 GHz in general.^{28,54,64} Thus, the regrown QD DFB lasers were utilized as an external modulated optical source to perform system demonstration without optical isolators. An

aggregate transmission capacity of 640 Gbit/s is achieved with a 64-Gbaud PAM-4 modulation and scaling beyond 1 Tbit/s is feasible (Figure 5d). Realizing high-quality MBE regrowth capability in GaAs-based materials is an important achievement here. It enables the possibility of monolithically integrating QD-DFB electro-absorption modulated laser (EML) devices by butt-coupled regrowth to spatially vary the bandgap for the modulator and the gain sections. The 40-Gbit/s transmission has already been reported using a conventional etching and regrowth process for the QW-based DFB-EML devices on native InP substrates.⁶⁵ This parallel effort can be leveraged in the epitaxial QD-based III–V on Si technology as well. For this path, managing etching and regrowth steps to achieve efficient optical coupling between the two waveguides, and accurate alignment of the absorption band edge of the EMLs with respect to the DFB lasing wavelengths is the subject of ongoing research.

Monolithic Integration with Si Waveguides. The previous section described what has been done by confining all functional devices to III–V layers where the high-index contrast, high-confinement, and low-loss Si waveguide is not used. This approach benefits from the lower substrate cost, large wafer size, lower thermal impedance of Si, and well-established wafer-scale CMOS fabrication in the Si industry. Currently, III–V growth on Si is being transferred from small Si pieces in research laboratories to industry oriented 150, 200, and 300 mm Si wafers. If the III–V growth can be done with high yield on large Si wafers, the integration processes on 300 mm Si wafers can provide a strong economic argument here. Meanwhile, from the learning curves obtained in QW devices, Si waveguides combined with III–V materials can push device performance well beyond the abilities of their monolithic counterparts.⁹ To achieve cointegration of QD lasers with other Si photonic components defined in the top Si layer of a SOI platform, A. Liu et al. proposed that the optical mode can be butt-coupled to a Si rib waveguide by selective area growth of III–V cavity onto a prepatterned SOI substrate. This approach is under active investigation. The III–V gain materials are deposited into trenches defined by the patterned oxide.⁶⁶ Leveraging the well-controlled growth techniques, the active region can be precisely aligned to the Si waveguides embedded in the oxide. This approach is the most economically viable approach to achieve monolithic integration between the III–V gain element and the Si waveguides as it makes the most use of the existing Si PIC technology. To further simplify the coupling, buffer-less selective growth of III–V on Si is being actively explored. QW nanoridge lasers have already been demonstrated under pulsed optical pumping,⁶⁷ incorporating QDs inside the same cavity should follow a similar learning curve. However, there is no clear roadmap yet to achieve efficient electrical injection as carriers would need to path through the resistive III–V/Si interface.

■ RELIABILITY OF QD LASERS EPITAXIALLY GROWN ON (001) SI

Reduction of Threading Dislocations. Monolithic integration through direct epitaxial growth is the ultimate solution for integrating light sources onto photonic chips. This more economically favorable option also provides the best natural heatsinking for laser operation. Yet, the electrically active crystalline defects originated from the material dissimilarities between the III–V and Si have posed severe limitations on device performance and reliability. Table 1

Table 1. Summary of the Main Aging Results in the Last Few Years^a

material generation	innovation	TDD (cm ⁻²)	TL position (nm)	pMD (cm ⁻³)	aging temp (°C)	extrapolated lifetime (h)			ref
						35 °C	60 °C	80 °C	
Gen I	GaP/Si to remove APD	2 × 10 ⁸	N/A	0	35	~800	N/A	N/A	68
Gen II	TCA to reduce TDD	7 × 10 ⁷	N/A	0	35	~20 K	~2 K	N/A	68
Gen III	SLS to reduce TDD	7 × 10 ⁶	N/A	0	35/60	>1 M	~2500	N/A	68
Gen IV	pMD for high T performance	7 × 10 ⁶	N/A	5 × 10 ¹⁷	60	~9 M	~70 K	<500	69
Gen V.A	TLs to block MDs	3 × 10 ⁷	180	5 × 10 ¹⁷	60	>1 M	>1 M	~11 K	70
Gen V.B		3 × 10 ⁷	80	5 × 10 ¹⁷	60/80	>1 M	~90 K	~30 K	70
Gen V.C		7 × 10 ⁶	180	5 × 10 ¹⁷	80	>1 M	~1 M	~100 K	71
Gen VI	ASG filter for record low TDD	1 × 10 ⁶	180	5 × 10 ¹⁷	80	>1 M	>1 M	>200 K	71

^aAll lifetime times are extracted after the aging trend stabilizes. The extrapolated lifetimes in bold are measured at that temperature, while the ones in black are estimate at higher or lower temperatures for comparison to other measured data based on a standard temperature acceleration model with an activation energy of 0.89 eV.¹¹ Each innovation (column 2) from Gen II onward is an add-on to the previous generation. N/A in columns 2 and 3 means the feature was not included in the laser. N/A in columns 8 and 9 means the laser did not maintain good lasing characteristics at those temperatures.

summarizes the progress in solving these problems and organizes the advances into six generations of heteroepitaxial lasers on silicon.

When a polar III–V material is grown directly on a nonpolar single-step (001) Si surface, the atom arrangement is swapped at the step edges, resulting in the formation of antiphase domains (APDs) at the interface. The APD problem has been resolved to a great extent by using the misoriented Si substrates together with high-temperature prebake treatment.⁷² More recently, some major breakthroughs have been made on CMOS compatible (001) Si substrate, either using a sophisticated Si surface preparation step,⁷³ selective patterning,^{33,74–77} or GaP buffer.⁷⁸ Notably, through careful surface preparation and well-tuned nucleation conditions, 300 mm GaP/Si templates with APD-free GaP grown on (001) Si are commercially available⁷⁸ and were used in the first-generation lasers (Table 1).

The most detrimental and yet unsolved issue of direct epitaxial growth is the high density of threading dislocations (TDs) originating from the high lattice constant mismatch. These extended defects propagate through all epitaxial layers and function as nonradiative recombination centers. Reducing the threading dislocation density (TDD) in the buffer layers has been the main, if not the sole, method to obtain high performance and long-lasting devices on Si.^{79–81} Various methods have been explored to reduce the TDD. Applying thermal treatments during the buffer growth (Gen II) and inserting dislocation filter layers (DFLs; Gen III) proved to be the most successful methods. TDD values as low as 7–9 × 10⁶ cm⁻² have been achieved with the use of thermal cyclic annealing (TCA) and strained layer superlattice (SLS) as the DFLs. For InAs QD lasers grown on (001) Si, when decreasing the TDD to the level of 7.6 × 10⁶ cm⁻², the extrapolated lifetime, defined as the time required to double the initial threshold current, exceeded 10000000 h at room temperature,⁶⁸ but only reached 5000 h at 60 °C.⁶⁹

Reduced reliability at elevated temperatures attributes to the enhanced carrier escape and nonradiative recombination rate. In the most technologically relevant QD material systems, namely, InAs/GaAs and InAs/InP, the valence band offset is small compared to kT, even at room temperature. Supplying extra holes in the active region with *p*-type modulation doping would compensate for the carrier escape at the expense of introducing additional nonradiative recombination and optical

absorption. At room temperature, *p*-type modulation doping proved to achieve a higher material gain, a lower slope efficiency, and a higher threshold current by both first-principal calculations and experimental measurements.^{27,40} At elevated temperatures where carrier escape is the dominating effect, the benefit of *p*-type modulation doping is more distinct. Incorporating a *p*-doping level of 5 × 10¹⁷ cm⁻³ within a 10 nm GaAs layer in the spacers between each dot layer, the extrapolated lifetime at 60 °C increases to approximately 70000 h, much higher than that of the 5000 h achieved with a UID active region (Gen IV).⁶⁹ Yet, this is still not sufficient for real-world data center applications, where the ambient temperature is at least 75 °C.

It is recently found that the efficiency of the DFL depends strongly on the indium composition and degree of relaxation. Using an “asymmetric graded filter” (ASG) structure instead of the traditional SLS, the degree of relaxation in the InGaAs DFL has been greatly improved to >80%, whereas the same metrics in a traditional InGaAs/GaAs superlattice DFL is only 15%. A surface TDD as low as 1 × 10⁶ cm⁻² has been achieved within 2.55 μm of III–V layers, as verified by both electron channeling contrast imaging (ECCI) and plan-view transmission electron microscopy (PVTEM; Figure 6).⁸²

Using Trapping Layers to Reduce Misfit Dislocations. The coefficient of thermal expansion (CTE) mismatch between III–V and Si causes strain during the cooldown after growth and thus causes dislocation migration. The CTE mismatch is used in thermal cycling to reduce TDD in the buffer layer, but this mechanism also results in wafer cracking and warping during the postgrowth cooling after depositing device layers. While neither of the effects are obvious on small wafers that are normally used in research laboratories, scaling to 300 mm wafers in real applications makes this a concern. In addition, CTE mismatch, together with the existence of TDs, is also responsible for the formation of MDs above and below the active region through a nonconventional mechanism, as shown in the schematic in Figure 7a,b.⁸³ During the postgrowth cooling process, the III–V layers experience tension from the CTE mismatch. The MDs at the III–V/Si interface, which are initially formed to relax the compressive stress during growth, would then “shrink” and drag the TD segments along. The InAs/InGaAs dot-in-a-well structure in the active region is stiffer due to alloy hardening. In this scenario, a portion of the TD would be trapped, leaving the MDs sandwiched in the

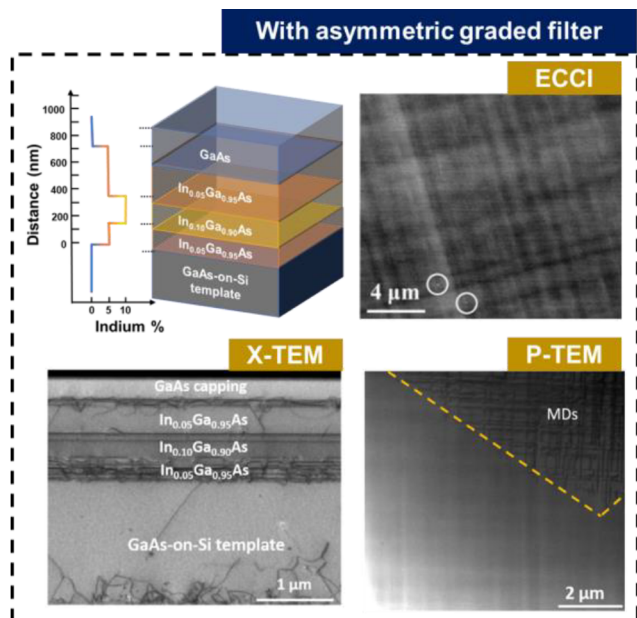


Figure 6. Schematic and the XTEM image of the asymmetric graded filter structure facilitating a higher level of relaxation in the InGaAs filters. The surface TDD is measured with ECCI (TD circled in white) and PVTEM. Reprinted with permission from ref 82. Copyright 2020 Wiley VCH.

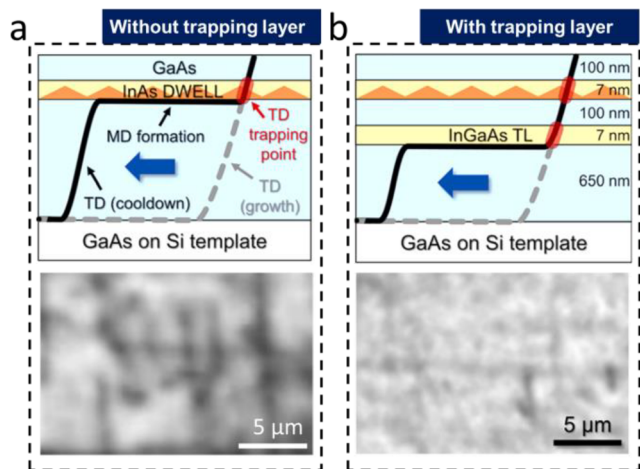


Figure 7. Schematic and the XTEM image of the asymmetric graded filter structure facilitating a higher level of relaxation in the InGaAs filters. The surface TDD is measured with ECCI (TD circled in white) and PVTEM. Schematic representation (upper) and monochromatic CL image (lower) of a QD structure (a) without and (b) with TL designs. The gray dashed lines represent the as-grown defect configuration, and the red ovals suggest pinning points in the active region and in the TL structure. Reproduced with permission from ref 83. Copyright 2020 AIP Publishing.

active region. Considering that the in-plane MDs possess a larger interaction area with the QDs compared to TDs, MDs can be more detrimental than TDs.⁸³ Selvidge et al. suggested utilizing the strain hardening effect and inserting thin strained QWs as trapping layers (TLs) above and below the active region to block the MDs away from the active region.⁸³ It has been experimentally confirmed via CL measurements that over 90% of the MDs are removed from the active region within a GaAs/AlGaAs-based laser stack on (001) Si, as is evident from

the lower images in Figure 7a,b (Gen V). It can be inferred that lower TDD would also help reduce the number of MDs, as the sources for such MDs are removed. Yet, achieving native substrate level TDD is unlikely due to kinetic limitations.⁸⁴ Thus, the introduction of TLs circumvents such limitations by tackling the problem directly.

Demonstration of High Temperature Robust Operation. Combining the low TDD GaAs virtual substrate with the asymmetric graded filter structure on (001) Si and inserting $\text{In}_{0.15}\text{Al}_{0.85}\text{As}$ and $\text{In}_{0.15}\text{Ga}_{0.85}\text{As}$ TLs in the *n*- and *p*-type cladding layers, respectively, the performance of the InAs QD laser has improved significantly (Gen VI).⁷¹ Figure 8a is the schematic of the laser cross-section, where the inserted TLs are placed 180 nm away from the active region. Figure 8b is the SEM image of the as-cleaved laser facet. The TL materials were chosen to avoid introducing additional electrical barriers and the composition was designed to match the QW composition in the active region. The threshold current and slope efficiency are both improved with this change and the characteristic temperature was increased from 88 to 167 K (without soldering to heat sinks; Figure 8c). This would enable much lower pumping level when operating at elevated temperatures. Figure 8d shows the 80 °C *L*–*I* evolutions for devices fabricated from three different types of material samples. Sample A (Gen IV) has no TL and was grown on a template with a TDD of $7.5 \times 10^6 \text{ cm}^{-2}$. As mentioned above, the same type of devices had an extrapolated lifetime of 70 000 h at 60 °C, but they experienced a 100% threshold increase within the first 3900 h of aging at 80 °C. Sample B has TLs inserted (Gen V) and is otherwise the same as Sample A. Sample C upgrades from Sample B by growing the same laser structure with TLs on the $1 \times 10^6 \text{ cm}^{-2}$ TDD template (Gen VI). All samples incorporate a *p*-type modulation doping of $5 \times 10^{17} \text{ cm}^{-3}$ for improved high-temperature performance. These three samples were grown sequentially in the MBE system and processed together. The *L*–*I* stability was improved drastically for both Sample B and Sample C, with a threshold increase of only 26.4% and 10.6%, respectively. The extrapolated lifetime is approximately 100 000 h for Sample B and more than 200 000 hours for Sample C. For the first time ever, robust CW operation at 80 °C has been achieved for the InAs QD laser, emitting near 1.3 μm, epitaxially grown on CMOS compatible (001) Si. Neither the asymmetric graded filter nor the trapping layers are unique to the GaAs-based material system. The analogies of such structures could be extended to other material systems, for example, the InAs/InP quantum dash system, where high performance broadband optical amplifiers,⁸⁵ mode-locked lasers,⁸⁶ superluminescent diodes,⁸⁷ and photodetectors⁸⁸ have been realized on a native InP substrate. Yet, the performance of the on-Si devices is less than ideal, possibly due to the insufficient reduction of the above-mentioned defects.

Postaging microscopy analysis done on an older generation of samples, aged at 60 °C, has revealed the mechanism of such inserted TLs.⁷⁰ The samples were grown on a template with $2 \times 10^7 \text{ cm}^{-2}$ TDD and the TLs were placed either 180 nm (TL180) or 80 nm (TL80) away from the active region. A sample with no TL was analyzed as well for comparison. In the PVTEMs in Figure 8e, the MDs near the active region in the sample with TLs have shown reduced climb, as is evident from the decreased waviness in the MDs. When MDs are pushed more into the doped region, the recombination enhanced dislocation climb (REDC) of the MDs is reduced due to the

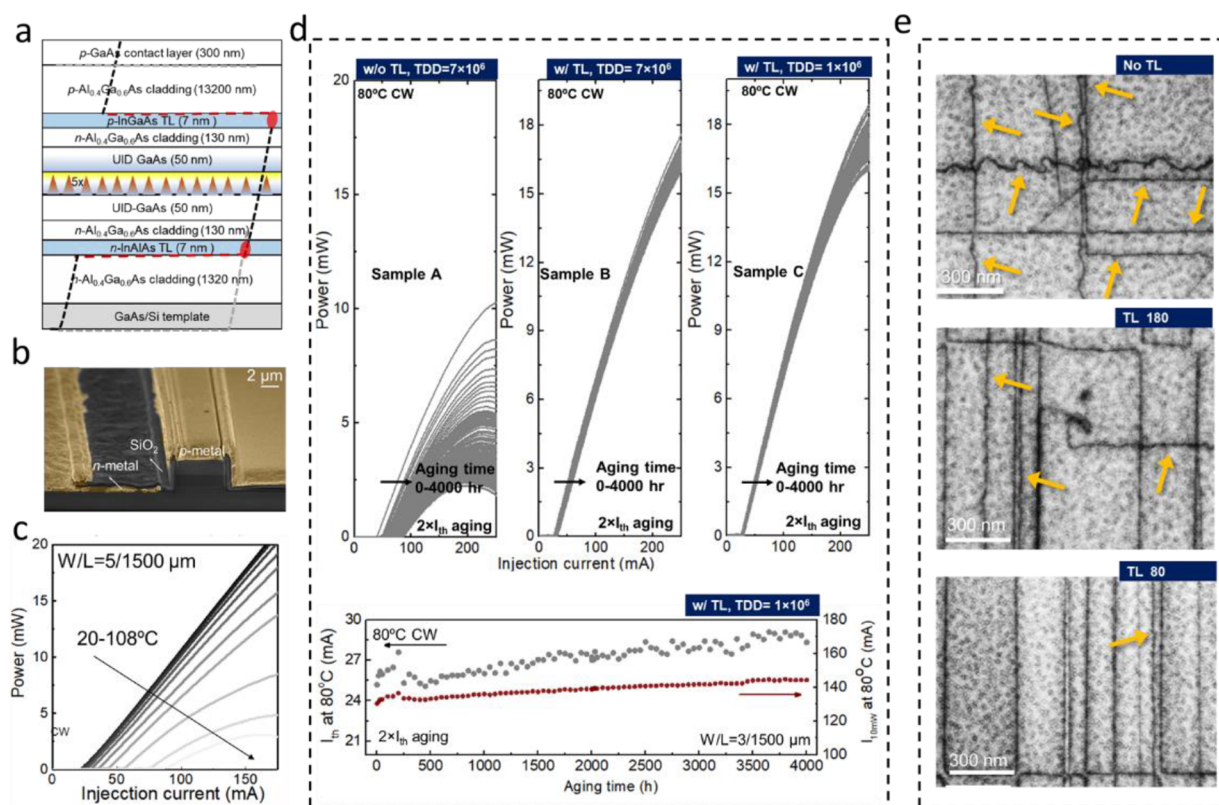


Figure 8. (a) Schematic of the laser stack with the inserted TLs 180 nm away from the active region. The MDs (red dashed lines) would form close to the TLs instead of the active region. (b) SEM images of the device being aged (c) Temperature-dependent $L-I$ curves of the best device incorporating the TL design on $1 \times 10^6 \text{ cm}^{-2}$ TDD GaAs-on-Si buffer. (d) $L-I$ curves evolution during the 4000 h aging at 80°C for different TL designs and TDD GaAs-on-Si buffer, the bottom figure shows aging data (at $80^\circ\text{C}/2 \times I_{th}$) for the hero device incorporating the TL design on $1 \times 10^6 \text{ cm}^{-2}$ TDD GaAs-on-Si buffer. (e) Postaging microscopy analysis for devices with different TL designs. Yellow arrows are pointing to the MDs showing signs of REDC. (a)–(d) Reprinted and adapted with permission from ref 71. Copyright 2021 The Optical Society. (e) Reproduced with permission from ref 70. Copyright 2021 AIP Publishing.

shortage of minority carriers. TL80 design proves to be more effective than the TL180 design with even less wavy MDs in the PVTEM image. Such a difference has been predicted by calculations.⁸⁹ The short TD segment in between the TLs and the active region grows increasingly unstable as it lengthens due to the excess stresses. Thus, TL80 provides a more mechanically stable laser structure. However, TL80 design renders a lower extrapolated lifetime compared to the TL180 design in the prolonged aging experiment. This discrepancy could be attributed to the fact that TL80 is in the less doped region. Optimizing the TL design for each specific laser structure is an ongoing effort. Nonetheless, TLs have been introduced as another very effective tool in managing crystalline defects in III–V materials epitaxially grown on Si.

CONCLUSIONS

After almost three decades of continuing development, QDs are now fulfilling their promise as superior light emitters. These advantages can be traced back to their discrete energy levels and symmetric gain spectra. Near native substrate level device performance and reliable operation at data center ambient temperatures have been achieved for the epitaxially grown QD lasers on Si. Low cost and high manufacturing scalability PICs via monolithic integration should be possible.

AUTHOR INFORMATION

Corresponding Author

Chen Shang – Materials Department, University of California–Santa Barbara, Santa Barbara, California 93106, United States; orcid.org/0000-0002-2577-9220; Email: shang00@ucsb.edu

Authors

Yating Wan – Department of Electronic and Computer Engineering, University of California–Santa Barbara, Santa Barbara, California 93106, United States; orcid.org/0000-0003-2157-2406

Jennifer Selvidge – Materials Department, University of California–Santa Barbara, Santa Barbara, California 93106, United States

Eamonn Hughes – Materials Department, University of California–Santa Barbara, Santa Barbara, California 93106, United States

Robert Herrick – Intel Corp., Santa Clara, California 95054, United States

Kunal Mukherjee – Department of Material Science and Engineering, Stanford University, Stanford, California 94305, United States

Jianan Duan – LTCl, Télécom Paris, Institut Polytechnique de Paris, 91120 Palaiseau, France; Center for High Technology Materials, University of New Mexico, Albuquerque, New Mexico 87106, United States

Frederic Grillot – *LTCI, Télécom Paris, Institut Polytechnique de Paris, 91120 Palaiseau, France; Center for High Technology Materials, University of New Mexico, Albuquerque, New Mexico 87106, United States*
Weng W. Chow – *Sandia National Laboratories, Albuquerque, New Mexico 87185-1086, United States*
John E. Bowers – *Department of Electronic and Computer Engineering, University of California–Santa Barbara, Santa Barbara, California 93106, United States*

Complete contact information is available at:
<https://pubs.acs.org/10.1021/acsp Photonics.1c00707>

Author Contributions

#C.S. and Y.W. contributed equally.

Notes

The authors declare no competing financial interest.

ACKNOWLEDGMENTS

We thank Gordon Keeler, Alan Liu, Justin Norman, David Harame, Matteo Meneghini, Robert Zhang, Rosalyn Koszica, Kaiyin Feng, Mario Dumont, Heming Huang, Bozhang Dong, and M. J. Kennedy for useful discussions and assistance. This research was supported by the U.S. Department of Defense under AIM Photonics (Air Force Contract FA8650-15-2-5220) and by the DARPA LUMOS (DARPA Contract HR001120C0142) and AFRL through AIM Photonics. This work was performed, in part, at the Center for Integrated Nanotechnologies, an Office of Science User Facility operated for the U.S. Department of Energy (DOE), Office of Science. The views and opinions expressed in this paper and those of the authors and do not reflect the official policy or position of the U.S. Air Force, Department of Defense, or the U.S. Government.

REFERENCES

- (1) Cisco. Global Cloud Index: Forecast and Methodology 2016–2021. 2018, <http://www.sdia.se/download/cisco-global-cloud-index-forecast-and-methodology-2016-2021-cisco-2018/>.
- (2) Patterson, D.; De Sousa, I.; Archard, L.-M. The Future of Packaging with Silicon Photonics. *Chip Scale Rev.* **2017**, 1–10.
- (3) Margalit, N.; Xiang, C.; Bowers, S. M.; Bjorlin, A.; Blum, R.; Bowers, J. E. Perspective on the Future of Silicon Photonics and Electronics. *Appl. Phys. Lett.* **2021**, *118* (22), 220501.
- (4) Rakowski, M. Silicon Photonics Platform for 50G Optical Interconnects. *Photonics Summit Work.* **2017**, 1–45.
- (5) Jones, R.; Doussiere, P.; Driscoll, J. B.; Lin, W.; Yu, H.; Akulova, Y.; Komljenovic, T.; Bowers, J. E. Heterogeneously Integrated InP/Silicon Photonics: Fabricating Fully Functional Transceivers. *IEEE Nanotechnol. Mag.* **2019**, *13* (2), 17–26.
- (6) Komljenovic, T.; Huang, D.; Pintus, P.; Tran, M. A.; Davenport, M. L.; Bowers, J. E. Photonic Integrated Circuits Using Heterogeneous Integration on Silicon; Photonic Integrated Circuits Using Heterogeneous Integration on Silicon. *Proc. IEEE* **2018**, *106*, 2246–2257.
- (7) Malik, A.; Liu, S.; Timurdogan, E.; Harrington, M.; Netherton, A.; Saeidi, M.; Blumenthal, D.; Theogarajan, L.; Watts, M.; Bowers, J. E. Low Power Consumption Silicon Photonics Datacenter Interconnects Enabled by a Parallel Architecture. *Optical Fiber Communication (OFC) Conference*, San Francisco, CA, U.S.A., 6–10 June, 2021, IEEE, 2021, DOI: 10.1143/jjap.40.6384.
- (8) Dai, D.; Bowers, J. E. Silicon-Based on-Chip Multiplexing Technologies and Devices for Peta-Bit Optical Interconnects. *Nanophotonics* **2014**, *3* (4–5), 283–311.
- (9) Liang, D.; Bowers, J. Recent Progress in Heterogeneous III-V-on-Silicon Photonic Integration. *Light Adv. Manuf.* **2021**, *2* (1), 1–25.
- (10) Arakawa, Y.; Sakaki, H. Multidimensional Quantum Well Laser and Temperature Dependence of Its Threshold Current. *Appl. Phys. Lett.* **1982**, *40* (11), 939–941.
- (11) Norman, J. C.; Jung, D.; Liu, A. Y.; Selvidge, J.; Mukherjee, K.; Bowers, J. E.; Herrick, R. W. Reliability of Lasers on Silicon Substrates for Silicon Photonics. In *Reliability of Semiconductor Lasers and Optoelectronic Devices*; Herrick, R., Ueda, O., Eds.; Elsevier, 2021; pp 239–272, DOI: 10.1016/B978-0-12-819254-2.00002-3.
- (12) Liu, Z.; Martin, M.; Baron, T.; Chen, S.; Seeds, A.; Penty, R.; White, I.; Liu, H.; Hantschmann, C.; Tang, M.; Lu, Y.; Park, J. S.; Liao, M.; Pan, S.; Sanchez, A.; Beanland, R. Origin of Defect Tolerance in InAs/GaAs Quantum Dot Lasers Grown on Silicon. *J. Lightwave Technol.* **2020**, *38* (2), 240–248.
- (13) Hantschmann, C.; Liu, Z.; Tang, M.; Chen, S.; Seeds, A. J.; Liu, H.; White, I. H.; Penty, R. V. Theoretical Study on the Effects of Dislocations in Monolithic III-V Lasers on Silicon. *J. Lightwave Technol.* **2020**, *38* (17), 4801–4807.
- (14) Tournie, E.; Cerutti, L.; Rodriguez, J.; Liu, H.; Wu, J.; Chen, S. Metamorphic III-V Semiconductor Lasers Grown on Silicon. *MRS Bull.* **2016**, *41*, 218–223.
- (15) Wan, Y.; Norman, J.; Bowers, J. *Quantum Dot Microcavity Lasers on Silicon Substrates*, 1st ed.; Elsevier Inc., 2019; Vol. 101, DOI: 10.1016/bs.semsem.2019.05.002.
- (16) Liu, A. Y.; Bowers, J. Photonic Integration with Epitaxial III–V on Silicon. *IEEE J. Sel. Top. Quantum Electron.* **2018**, *24* (6), 1.
- (17) Norman, J. C.; Jung, D.; Wan, Y.; Bowers, J. E. Perspective: The Future of Quantum Dot Photonic Integrated Circuits. *APL Photonics* **2018**, *3* (3), 030901.
- (18) Bimberg, D.; Grundmann, M.; Heinrichsdorff, F.; Ledentsov, N. N.; Ustinov, V. M.; Zhukov, A. E.; Kovsh, A. R.; Maximov, M. V.; Shernyakov, Y. M.; Volovik, B. V.; Tsatsul'nikov, A. F.; Kop'ev, P. S.; Alferov, Z. I. Quantum Dot Lasers: Breakthrough in Optoelectronics. *Thin Solid Films* **2000**, *367* (1–2), 235–249.
- (19) Wan, Y.; Norman, J.; Liu, S.; Liu, A.; Bowers, J. E. Quantum Dot Lasers and Amplifiers on Silicon: Recent Advances and Future Developments. *IEEE Nanotechnol. Mag.* **2021**, *15* (2), 8–22.
- (20) Asryan, L. V.; Suris, R. A. Theory of Threshold Characteristics of Semiconductor Quantum Dot Lasers. *Semiconductors* **2004**, *38* (1), 1–22.
- (21) Norman, J. C.; Jung, D.; Zhang, Z.; Wan, Y.; Liu, S.; Shang, C.; Herrick, R. W.; Chow, W. W.; Gossard, A. C.; Bowers, J. E. A Review of High-Performance Quantum Dot Lasers on Silicon. *IEEE J. Quantum Electron.* **2019**, *55* (2), 1.
- (22) Chow, W. W.; Zhang, Z.; Norman, J. C.; Liu, S.; Bowers, J. E. On Quantum-Dot Lasing at Gain Peak with Linewidth Enhancement Factor $\alpha_H = 0$. *APL Photonics* **2020**, *5* (2), 026101.
- (23) Chow, W. W.; Liu, A. Y.; Gossard, A. C.; Bowers, J. E. Extraction of Inhomogeneous Broadening and Nonradiative Losses in InAs Quantum-Dot Lasers. *Appl. Phys. Lett.* **2015**, *107* (17), 171106.
- (24) Selvidge, J.; Norman, J.; Salmon, M. E.; Hughes, E. T.; Bowers, J. E.; Herrick, R.; Mukherjee, K. Non-Radiative Recombination at Dislocations in InAs Quantum Dots Grown on Silicon. *Appl. Phys. Lett.* **2019**, *115* (13), 131102.
- (25) Kim, J. K.; Strand, T. A.; Naone, R. L.; Coldren, L. A. Design Parameters for Lateral Carrier Confinement in Quantum-Dot Lasers. *Appl. Phys. Lett.* **1999**, *74* (19), 2752–2754.
- (26) Strand, T. A.; Thibeault, B. J.; Coldren, L. A. Reduced Lateral Carrier Diffusion for Improved Miniature Semiconductor Lasers. *J. Appl. Phys.* **1997**, *81* (8), 3377–3381.
- (27) Norman, J. C.; Jung, D.; Zhang, Z.; Wan, Y.; Liu, S.; Shang, C.; Herrick, R. W.; Chow, W. W.; Gossard, A. C.; Bowers, J. E. A Review of High-Performance Quantum Dot Lasers on Silicon. *IEEE J. Quantum Electron.* **2019**, *55* (2), 1–11.
- (28) Wan, Y.; Inoue, D.; Jung, D.; Norman, J. C.; Shang, C.; Gossard, A. C.; Bowers, J. E. Directly Modulated Quantum Dot Lasers on Silicon with a Milliampere Threshold and High Temperature Stability. *Photonics Res.* **2018**, *6* (8), 776.
- (29) Wan, Y.; Norman, J.; Li, Q.; Kennedy, M. J.; Liang, D.; Zhang, C.; Huang, D.; Zhang, Z.; Liu, A. Y.; Torres, A.; Jung, D.; Gossard, A.

- C.; Hu, E. L.; Lau, K. M.; Bowers, J. E. 13 Mm Submilliamp Threshold Quantum Dot Micro-Lasers on Si. *Optica* **2017**, *4* (8), 940.
- (30) Chen, S.; Li, W.; Wu, J.; Jiang, Q.; Tang, M.; Shutts, S.; Elliott, S. N.; Sobiesierski, A.; Seeds, A. J.; Ross, L.; Smowton, P. M.; Liu, H. Electrically Pumped Continuous-Wave III-V Quantum Dot Lasers on Silicon. *Nat. Photonics* **2016**, *10* (5), 307–311.
- (31) Liu, A. Y.; Zhang, C.; Norman, J.; Snyder, A.; Lubyshev, D.; Fastenau, J. M.; Liu, A. W. K.; Gossard, A. C.; Bowers, J. E. High Performance Continuous-Wave $1.3\ \mu\text{m}$ Quantum Dot Lasers on Silicon. *Appl. Phys. Lett.* **2014**, *104*, 041104.
- (32) Jung, D.; Norman, J.; Kennedy, M. J.; Shang, C.; Shin, B.; Wan, Y.; Gossard, A. C.; Bowers, J. E. High Efficiency Low Threshold Current $1.3\ \mu\text{m}$ InAs Quantum Dot Lasers on on-Axis (001) GaP/Si. *Appl. Phys. Lett.* **2017**, *111* (12), 122107.
- (33) Norman, J.; Kennedy, M. J.; Selvidge, J.; Li, Q.; Wan, Y.; Liu, A. Y.; Callahan, P. G.; Echlin, M. P.; Pollock, T. M.; Lau, K. M.; Gossard, A. C.; Bowers, J. E. Electrically Pumped Continuous Wave Quantum Dot Lasers Epitaxially Grown on Patterned, on-Axis (001) Si. *Opt. Express* **2017**, *25* (4), 3927.
- (34) Kageyama, T.; Nishi, K.; Yamaguchi, M.; Mochida, R.; Maeda, Y.; Takemasa, K.; Tanaka, Y.; Yamamoto, T.; Sugawara, M.; Arakawa, Y. Extremely High Temperature (220°C) Continuous-Wave Operation of 1300-Nm -Range Quantum-Dot Lasers. *2011 Conf. Lasers Electro-Optics Eur. 12th Eur. Quantum Electron. Conf.* **2011**, 1–1.
- (35) Zhang, Z.; Jung, D.; Norman, J. C.; Chow, W. W.; Bowers, J. E. Linewidth Enhancement Factor in InAs/GaAs Quantum Dot Lasers and Its Implication in Isolator-Free and Narrow Linewidth Applications. *IEEE J. Sel. Top. Quantum Electron.* **2019**, *25* (6), 1–9.
- (36) Rideout, W.; Yu, B.; LaCourse, J.; York, P. K.; Beernink, K. J.; Coleman, J. J. Measurement of the Carrier Dependence of Differential Gain, Refractive Index, and Linewidth Enhancement Factor in Strained-Layer Quantum Well Lasers. *Appl. Phys. Lett.* **1990**, *56* (8), 706–708.
- (37) Schwarz, U. T.; Sturm, E.; Wegscheider, W.; Kümmler, V.; Lell, A.; Härle, V. Optical Gain, Carrier-Induced Phase Shift, and Linewidth Enhancement Factor in InGaN Quantum Well Lasers. *Appl. Phys. Lett.* **2003**, *83* (20), 4095–4097.
- (38) Osinski, M.; Buus, J. Linewidth Broadening Factor in Semiconductor Lasers—An Overview. *IEEE J. Quantum Electron.* **1987**, *23* (1), 9–29.
- (39) Helms, J.; Petermann, K. A Simple Analytic Expression for the Stable Operation Range of Laser Diodes with Optical Feedback. *IEEE J. Quantum Electron.* **1990**, *26* (5), 833–836.
- (40) Zhang, Z.; Jung, D.; Norman, J. C.; Patel, P.; Chow, W. W.; Bowers, J. E. Effects of Modulation p Doping in InAs Quantum Dot Lasers on Silicon. *Appl. Phys. Lett.* **2018**, *113* (6), 061105.
- (41) Huang, H.; Duan, J.; Jung, D.; Liu, A. Y.; Zhang, Z.; Norman, J.; Bowers, J. E.; Grillot, F. Analysis of the Optical Feedback Dynamics in InAs/GaAs Quantum Dot Lasers Directly Grown on Silicon. *J. Opt. Soc. Am. B* **2018**, *35* (11), 2780.
- (42) Duan, J.; Huang, H.; Dong, B.; Jung, D.; Norman, J. C.; Bowers, J. E.; Grillot, F. $1.3\text{-}\mu\text{m}$ Reflection Insensitive InAs/GaAs Quantum Dot Lasers Directly Grown on Silicon. *IEEE Photonics Technol. Lett.* **2019**, *31* (5), 345–348.
- (43) Dong, B.; Chen, J.; Lin, F.; Norman, J. C.; Bowers, J. E.; Grillot, F. Dynamic and Nonlinear Properties of Epitaxial Quantum-Dot Lasers on Silicon Operating under Longand Short-Cavity Feedback Conditions for Photonic Integrated Circuits. *Phys. Rev. A: At, Mol, Opt. Phys.* **2021**, *103*, na.
- (44) Grillot, F.; Duan, J.; Dong, B.; Huang, H.; Liu, S.; Chow, W. W.; Norman, J. C.; Bowers, J. E. Quantum Dot Lasers Based Photonics Integrated Circuits. *2020 IEEE Photonics Conf. IPC 2020 - Proc.* **2020**, *1*, 1.
- (45) Duan, J.; Chow, W. W.; Dong, B.; Huang, H.; Liu, S.; Norman, J. C.; Bowers, J. E.; Grillot, F. Enhanced Optical Nonlinearities in Epitaxial Quantum Dots Lasers on Silicon for Future Photonic Integrated Systems. *arXiv:2106.10871 [physics.optics]* **2021**, 10871, na.
- (46) Chow, W. W.; Liu, S.; Zhang, Z.; Bowers, J. E.; Sargent, M. Multimode Description of Self-Mode Locking in a Single-Section Quantum-Dot Laser. *Opt. Express* **2020**, *28* (4), 5317.
- (47) Wang, Z.-H.; Wei, W.-Q.; Feng, Q.; Wang, T.; Zhang, J.-J. InAs/GaAs Quantum Dot Single-Section Mode-Locked Lasers on Si (001) with Optical Self-Injection Feedback. *Opt. Express* **2021**, *29* (2), 674.
- (48) Liu, S.; Jung, D.; Norman, J.; Kennedy, M.; Gossard, A. C.; Bowers, J. E. 490 Fs Pulse Generation from Passively Mode-Locked Single Section Quantum Dot Laser Directly Grown on on-Axis GaP/Si. *Electron. Lett.* **2018**, *54* (7), 432–433.
- (49) Wan, Y.; Xiang, C.; Guo, J.; Koscica, R.; Kennedy, M.; Selvidge, J.; Zhang, Z.; Chang, L.; Xie, W.; Huang, D.; Gossard, A. C.; Bowers, J. E. High Speed Evanescent Quantum-Dot Lasers on Si. *Laser Photonics Rev.* **2021**, 2100057.
- (50) Wan, Y.; Norman, J. C.; Tong, Y.; Kennedy, M. J.; He, W.; Selvidge, J.; Shang, C.; Dumont, M.; Malik, A.; Tsang, H. K.; Gossard, A. C.; Bowers, J. E. $1.3\ \text{Mm}$ Quantum Dot-Distributed Feedback Lasers Directly Grown on (001) Si. *Laser Photonics Rev.* **2020**, *14* (7), 2000037.
- (51) Fang, A. W.; Park, H.; Cohen, O.; Jones, R.; Paniccia, M. J.; Bowers, J. E. Electrically Pumped Hybrid AlGaInAs-Silicon Evanescent Laser. *Opt. Express* **2006**, *14* (20), 9203.
- (52) Khan, M. Z. M.; Ng, T. K.; Ooi, B. S. Self-Assembled InAs/InP Quantum Dots and Quantum Dashes: Material Structures and Devices. *Prog. Quantum Electron.* **2014**, *38* (6), 237–313.
- (53) Kurczveil, G.; Liang, D.; Fiorentino, M.; Beausoleil, R. G. Robust Hybrid Quantum Dot Laser for Integrated Silicon Photonics. *Opt. Express* **2016**, *24* (14), 16167.
- (54) Zhang, C.; Liang, D.; Kurczveil, G.; Descos, A.; Beausoleil, R. G. Hybrid Quantum-Dot Microring Laser on Silicon. *Optica* **2019**, *6* (9), 1145.
- (55) Uvin, S.; Kumari, S.; De Groote, A.; Verstyuyt, S.; Lepage, G.; Verheyen, P.; Van Campenhout, J.; Morthier, G.; Van Thourhout, D.; Roelkens, G. $13\ \text{Mm}$ InAs/GaAs Quantum Dot DFB Laser Integrated on a Si Waveguide Circuit by Means of Adhesive Die-to-Wafer Bonding. *Opt. Express* **2018**, *26* (14), 18302.
- (56) Liang, D.; Srinivasan, S.; Descos, A.; Zhang, C.; Kurczveil, G.; Huang, Z.; Beausoleil, R. High-Performance QD DFB Laser on Silicon for High-Speed Modulations. *Optica* **2021**, *8* (5), 591–593.
- (57) Wan, Y.; Zhang, S.; Norman, J. C.; Kennedy, M. J.; He, W.; Tong, Y.; Shang, C.; He, J. J.; Tsang, H. K.; Gossard, A. C.; Bowers, J. E. Directly Modulated Single-Mode Tunable Quantum Dot Lasers at $1.3\ \text{Mm}$. *Laser Photonics Rev.* **2020**, *14* (3), 1900348.
- (58) Ding, Y.-Y.; Lv, Z.-R.; Zhang, Z.-K.; Yuan, H.-H.; Yang, T. Single Longitudinal Mode GaAs-Based Quantum Dot Laser with Refractive Index Perturbation. *Appl. Opt.* **2020**, *59* (6), 1648.
- (59) Rong, H.; Jones, R.; Liu, A.; Cohen, O.; Hak, D.; Fang, A.; Paniccia, M. A Continuous-Wave Raman Silicon Laser. *Nature* **2005**, *433* (7027), 725–728.
- (60) Malik, A.; Guo, J.; Tran, M. A.; Kurczveil, G.; Liang, D.; Bowers, J. E. Widely Tunable, Heterogeneously Integrated Quantum-Dot O-Band Lasers on Silicon. *Photonics Res.* **2020**, *8* (10), 1551.
- (61) Wan, Y.; Zhang, S.; Norman, J. C.; Kennedy, M. J.; He, W.; Liu, S.; Xiang, C.; Shang, C.; He, J.-J.; Gossard, A. C.; Bowers, J. E. Tunable Quantum Dot Lasers Grown Directly on Silicon. *Optica* **2019**, *6* (11), 1394.
- (62) Srinivasan, S.; Tossoun, B.; Kurczveil, G.; Huang, Z.; Liang, D.; Beausoleil, R. $160\ \text{Gb/s}$ Optical Link Using Quantum-Dot Comb Laser Source and SiGe APD. *Proc. Cust. Integr. Circuits Conf.* **2020**, 1.
- (63) Zhang, Z.; Norman, J. C.; Liu, S.; Malik, A.; Bowers, J. E. Integrated Dispersion Compensated Mode-Locked Quantum Dot Laser. *Photonics Res.* **2020**, *8* (9), 1428.
- (64) Fiore, A.; Markus, A. Differential Gain and Gain Compression in Quantum-Dot Lasers. *IEEE J. Quantum Electron.* **2007**, *43* (4), 287–294.
- (65) Kobayashi, W.; Fujiwara, N.; Tadokoro, T. Uncooled Operation of $10\text{-}/40\text{-Gbit/s}$ Integrated with Distributed Feedback Laser. *NTT Technol. Rev.* **2010**, *8* (8), na.

- (66) Liu, A. Y.; Srinivasan, S.; Norman, J.; Gossard, A. C.; Bowers, J. E. Quantum Dot Lasers for Silicon Photonics. *Photonics Res.* **2015**, *3* (5), B1–B9.
- (67) Shi, Y.; Wang, Z.; Van Campenhout, J.; Pantouvakis, M.; Guo, W.; Kunert, B.; Van Thourhout, D. Optical Pumped InGaAs/GaAs Nano-Ridge Laser Epitaxially Grown on a Standard 300-Mm Si Wafer. *Optica* **2017**, *4* (12), 1468.
- (68) Jung, D.; Herrick, R.; Norman, J.; Turnlund, K.; Jan, C.; Feng, K.; Gossard, A. C.; Bowers, J. E. Impact of Threading Dislocation Density on the Lifetime of InAs Quantum Dot Lasers on Si. *Appl. Phys. Lett.* **2018**, *112* (15), 153507.
- (69) Jung, D.; Norman, J.; Wan, Y.; Liu, S.; Herrick, R.; Selvidge, J.; Mukherjee, K.; Gossard, A. C.; Bowers, J. E. Recent Advances in InAs Quantum Dot Lasers Grown on On-Axis (001) Silicon by Molecular Beam Epitaxy. *Phys. Status Solidi A* **2019**, *216* (1), 1800602.
- (70) Selvidge, J.; Hughes, E. T.; Norman, J. C.; Shang, C.; Kennedy, M. J.; Dumont, M.; Nethererton, A. M.; Zhang, Z.; Herrick, R. W.; Bowers, J. E.; Mukherjee, K. Reduced Dislocation Growth Leads to Long Lifetime InAs Quantum Dot Lasers on Silicon at High Temperatures. *Appl. Phys. Lett.* **2021**, *118* (19), 192101.
- (71) Shang, C.; Hughes, E.; Wan, Y.; Dumont, M.; Koscica, R.; Selvidge, J.; Herrick, R.; Gossard, A. C.; Mukherjee, K.; Bowers, J. E. High Temperature Reliable Quantum-Dot Lasers on Si with Misfit and Threading Dislocation Filters. *Optica* **2021**, *8* (5), 749.
- (72) Akiyama, M.; Kawarada, Y.; Kaminishi, K. Growth of GaAs on Si by MOVCD. *J. Cryst. Growth* **1984**, *68*, 21–26.
- (73) Chen, S.; Liao, M.; Tang, M.; Wu, J.; Martin, M.; Baron, T.; Seeds, A.; Liu, H. Electrically Pumped Continuous-Wave 1.3 Mm InAs/GaAs Quantum Dot Lasers Monolithically Grown on on-Axis Si (001) Substrates. *Opt. Express* **2017**, *25* (5), 4632–4639.
- (74) Li, Q.; Ng, K. W.; Lau, K. M. Growing Antiphase-Domain-Free GaAs Thin Films out of Highly Ordered Planar Nanowire Arrays on Exact (001) Silicon. *Appl. Phys. Lett.* **2015**, *106* (7), 072105.
- (75) Zhang, B.; Wei, W. Q.; Wang, J. H.; Wang, H. L.; Zhao, Z.; Liu, L.; Cong, H.; Feng, Q.; Liu, H.; Wang, T.; Zhang, J. J. O-Band InAs/GaAs Quantum-Dot Microcavity Laser on Si (001) Hollow Substrate by in-Situ Hybrid Epitaxy. *AIP Adv.* **2019**, *9* (1), 015331.
- (76) Wan, Y.; Jung, D.; Norman, J.; Shang, C.; MacFarlane, I.; Li, Q.; Kennedy, M. J.; Gossard, A. C.; Lau, K. M.; Bowers, J. E. O-Band Electrically Injected Quantum Dot Micro-Ring Lasers on on-Axis (001) GaP/Si and V-Groove Si. *Opt. Express* **2017**, *25* (22), 26853.
- (77) Wan, Y.; Bowers, J. E.; Shang, C.; Norman, J.; Shi, B.; Li, Q.; Collins, N.; Dumont, M.; Lau, K. M.; Gossard, A. C. Low Threshold Quantum Dot Lasers Directly Grown on Unpatterned Quasi-Nominal (001) Si. *IEEE J. Sel. Top. Quantum Electron.* **2020**, *26* (2), 1–9.
- (78) Németh, I.; Kunert, B.; Stolz, W.; Volz, K. Heteroepitaxy of GaP on Si: Correlation of Morphology, Anti-Phase-Domain Structure and MOVPE Growth Conditions. *J. Cryst. Growth* **2008**, *310* (7–9), 1595–1601.
- (79) Kwoen, J.; Jang, B.; Lee, J.; Kageyama, T.; Watanabe, K.; Arakawa, Y. All MBE Grown InAs/GaAs Quantum Dot Lasers on on-Axis Si (001). *Opt. Express* **2018**, *26* (9), 11568.
- (80) Lee, A. D.; Qi Jiang; Mingchu Tang; Yunyan Zhang; Seeds, A. J.; Huiyun Liu. InAs/GaAs Quantum-Dot Lasers Monolithically Grown on Si, Ge, and Ge-on-Si Substrates. *IEEE J. Sel. Top. Quantum Electron.* **2013**, *19* (4), 1901107.
- (81) Tang, M.; Chen, S.; Wu, J.; Jiang, Q.; Dorogan, V. G.; Benamara, M.; Mazur, Y. I.; Salamo, G. J.; Seeds, A.; Liu, H. 13-Mm InAs/GaAs Quantum-Dot Lasers Monolithically Grown on Si Substrates Using InAlAs/GaAs Dislocation Filter Layers. *Opt. Express* **2014**, *22* (10), 11528.
- (82) Shang, C.; Selvidge, J.; Hughes, E.; Norman, J. C.; Taylor, A. A.; Gossard, A. C.; Mukherjee, K.; Bowers, J. E. A Pathway to Thin GaAs Virtual Substrate on On-Axis Si (001) with Ultralow Threading Dislocation Density. *Phys. Status Solidi A* **2021**, *218* (3), 2000402.
- (83) Selvidge, J.; Norman, J.; Hughes, E. T.; Shang, C.; Jung, D.; Taylor, A. A.; Kennedy, M. J.; Herrick, R.; Bowers, J. E.; Mukherjee, K. Defect Filtering for Thermal Expansion Induced Dislocations in III-V Lasers on Silicon. *Appl. Phys. Lett.* **2020**, *117* (12), 122101.
- (84) Ward, T.; Sánchez, A. M.; Tang, M.; Wu, J.; Liu, H.; Dunstan, D. J.; Beanland, R. Design Rules for Dislocation Filters. *J. Appl. Phys.* **2014**, *116* (6), 063508.
- (85) Eyal, O.; Willinger, A.; Mikhelashvili, V.; Banyoudeh, S.; Schnabel, F.; Sichkovsky, V.; Reithmaier, J. P.; Eisenstein, G. High Performance 1550 Nm Quantum Dot Semiconductor Optical Amplifiers Operating at 25–100°C. *2018 Opt. Fiber Commun. Conf. Expo. OFC 2018 - Proc.* **2018**, W3F.3.
- (86) Panapakkm, V.; Anthur, A. P.; Vujicic, V.; Zhou, R.; Gaimard, Q.; Merghem, K.; Aubin, G.; Lelarge, F.; Viktorov, E. A.; Barry, L. P.; Ramdane, A. Amplitude and Phase Noise of Frequency Combs Generated by Single-Section InAs/InP Quantum-Dash-Based Passively and Actively Mode-Locked Lasers. *IEEE J. Quantum Electron.* **2016**, *52* (11), 1.
- (87) Ooi, B. S.; Susanto Djie, H.; Wang, Y.; Tan, C. L.; Hwang, J. C. M.; Fang, X. M.; Fastenau, J. M.; Liu, A. W. K.; Dang, G. T.; Chang, W. H. Quantum Dashes on Inp Substrate for Broadband Emitter Applications. *IEEE J. Sel. Top. Quantum Electron.* **2008**, *14* (4), 1230–1238.
- (88) Wan, Y.; Shang, C.; Huang, J.; Xie, Z.; Jain, A.; Norman, J.; Chen, B.; Gossard, A. C.; Bowers, J. E. Low Dark Current 1.55 Micrometer InAs Quantum Dash Waveguide Photodiodes. *ACS Nano* **2020**, *14* (3), 3519–3527.
- (89) Mukherjee, K.; Selvidge, J.; Hughes, E.; Norman, J. C.; Shang, C.; Herrick, R.; Bowers, J. E. On the Formation of Misfit Dislocations in InAs Quantum Dot Lasers on Silicon. 2021, Submitted for publication.

NOTE ADDED AFTER ASAP PUBLICATION

After ASAP publication on August 11, 2021, some of the extrapolated lifetimes were adjusted. The corrected version was reposted on August 13, 2021.